Explaining Seasonal Fluctuations of Measles in Niger Using Nighttime Lights Imagery

N. Bharti, *et al.*

Science **334**, 1424 (2011);
DOI: 10.1126/science.1210554

tinct from that of GFP (Fig. 4B). At 3 days of culture, all organoids were LacZ negative, but by 7 days >20% of the organoids expressed β-Gal (Fig. 4, C and D), and by 21 days 100% (47/47) expressed β-Gal (Fig. 4D), demonstrating that *Lgr5*-positive cells can give rise to *Hopx*-expressing cells in vitro. In vivo, fate mapping of *Lgr5* cells with $Hopx^{LacZ/+}$;$Lgr5^{EGFP\text{-}ERCre/+}$;$R26^{mT\text{-}mG/+}$ mice, 5 months after a 5-day tamoxifen pulse, revealed entire crypt-villus structures that express membrane-bound GFP, including cells at the +4 position that simultaneously expressed β-Gal, indicating that they were derived from *Lgr5*-positive precursors (Fig. 4E). We also prepared near single-cell suspensions of crypts from $Hopx^{LacZ/+}$;$Lgr5^{EGFP\text{-}ERCre/+}$;$R26^{tdTomato/+}$ ($Hopx^{LacZ/+}$;$Lgr5^{EGFP\text{-}ERCre/+}$;$R26^{Tom/+}$) mice either 18 hours, 5 days, or 10 days after a single pulse of tamoxifen and analyzed the cells for LacZ and tdTomato expression. Eighteen hours after induction, we found no LacZ and tdTomato double-positive cells, consistent with *Hopx*-expressing cells being distinct from *Lgr5*-positive cells. However, over the ensuing 10 days, double-positive cells emerged, confirming that *Lgr5*-positive cells can give rise to *Hopx*-expressing, +4 cells (Fig. 4F).

Our results provide experimental evidence to support a proposed model (*2*) in which slowly cycling ISCs at the +4 position dynamically interconvert with more rapidly cycling ISCs at the crypt base (CBCs). Both populations display properties of self-renewal and are multipotent, consistent with stem cell identity. These findings help to reconcile prior controversy in the field and suggest that adult organ-specific stem cells in distinct niches can regenerate one another. Further elucidation of the unique properties of each stem cell population and the signals that regulate interconversion will be likely to inform gastrointestinal pathophysiology and stem cell biology in the future.

References and Notes

1. R. G. Vries, M. Huch, H. Clevers, *Mol. Oncol.* **4**, 373 (2010).
2. L. Li, H. Clevers, *Science* **327**, 542 (2010).
3. C. S. Potten, L. Kovacs, E. Hamilton, *Cell Tissue Kinet.* **7**, 271 (1974).
4. E. Sangiorgi, M. R. Capecchi, *Nat. Genet.* **40**, 915 (2008).
5. N. Barker *et al.*, *Nature* **449**, 1003 (2007).
6. M. Bjerknes, H. Cheng, *Gastroenterology* **116**, 7 (1999).
7. H. Cheng, C. P. Leblond, *Am. J. Anat.* **141**, 537 (1974).
8. C. S. Potten, S. E. Al-Barwari, W. J. Hume, J. Searle, *Cell Tissue Kinet.* **10**, 557 (1977).
9. D. T. Breault *et al.*, *Proc. Natl. Acad. Sci. U.S.A.* **105**, 10420 (2008).
10. R. K. Montgomery *et al.*, *Proc. Natl. Acad. Sci. U.S.A.* **108**, 179 (2011).
11. H. Tian *et al.*, *Nature* **478**, 255 (2011).
12. F. Chen *et al.*, *Cell* **110**, 713 (2002).
13. C. H. Shin *et al.*, *Cell* **110**, 725 (2002).
14. A. De Toni *et al.*, *Neural Dev.* **3**, 13 (2008).
15. C. S. Potten, G. Owen, D. Booth, *J. Cell Sci.* **115**, 2381 (2002).
16. X. C. He *et al.*, *Nat. Genet.* **36**, 1117 (2004).
17. P. Soriano, *Nat. Genet.* **21**, 70 (1999).
18. Materials and methods are available as supporting material on *Science* Online.
19. T. Sato *et al.*, *Nature* **459**, 262 (2009).
20. F. Relaix, D. Rocancourt, A. Mansouri, M. Buckingham, *Nature* **435**, 948 (2005).
21. C. S. Potten *et al.*, *Differentiation* **71**, 28 (2003).
22. L. G. van der Flier, A. Haegebarth, D. E. Stange, M. van de Wetering, H. Clevers, *Gastroenterology* **137**, 15 (2009).
23. L. G. van der Flier *et al.*, *Cell* **136**, 903 (2009).
24. T. Sato *et al.*, *Nature* **469**, 415 (2011).

Acknowledgments: We thank the Epstein laboratory for helpful discussions; C. J. Lengner, A. Padmanabhan, N. Singh, and K. S. Zaret for critical reading of the manuscript; and the Penn Flow Cytometry core and C. Pletcher for assistance with FACS experiments. This work was supported by an American Heart Association Physician-Scientist/Postdoctoral fellowship to R.J. (AHA 0825548D) and funds from the NIH (R01 HL071546, U01 HL100405), the Spain fund for Regenerative Medicine, and W. W. Smith Endowed Chair to J.A.E.

Supporting Online Material

www.sciencemag.org/cgi/content/full/science.1213214/DC1
Materials and Methods
Figs. S1 to S7
References (*25*–*29*)

26 August 2011; accepted 28 October 2011
Published online 10 November 2011;
10.1126/science.1213214

Explaining Seasonal Fluctuations of Measles in Niger Using Nighttime Lights Imagery

N. Bharti,[1,2]* A. J. Tatem,[3,4,10] M. J. Ferrari,[5,6] R. F. Grais,[7,8] A. Djibo,[9] B. T. Grenfell[1,2,10]

Measles epidemics in West Africa cause a significant proportion of vaccine-preventable childhood mortality. Epidemics are strongly seasonal, but the drivers of these fluctuations are poorly understood, which limits the predictability of outbreaks and the dynamic response to immunization. We show that measles seasonality can be explained by spatiotemporal changes in population density, which we measure by quantifying anthropogenic light from satellite imagery. We find that measles transmission and population density are highly correlated for three cities in Niger. With dynamic epidemic models, we demonstrate that measures of population density are essential for predicting epidemic progression at the city level and improving intervention strategies. In addition to epidemiological applications, the ability to measure fine-scale changes in population density has implications for public health, crisis management, and economic development.

Despite the interruption of endemic measles transmission in some parts of the industrialized world, this vaccine-preventable disease remains a major cause of childhood mortality in developing countries. Recurrent outbreaks of measles in low-income nations reflect the challenges of achieving and maintaining high vaccination levels with limited public health infrastructure. Major epidemics still occur, often with marked seasonal fluctuations in measles incidence (*1*, *2*), across a wide range of environmental conditions (*3*–*5*). Seasonal fluctuations in measles transmission rates are generally hypothesized to be a result of changes in population density (*1*), but it has long been challenging to assess these relations explicitly (*6*, *7*). Deciphering the drivers of epidemic seasonality is an important prerequisite to predicting the spread of infection and increasing the impact of immunization measures (*8*, *9*).

Population density is a major determinant of contact rates and transmission of directly transmitted infections. Within a spatial unit, density is commonly presented as a static, uniform quantity, although it may vary with time and across space. For human populations, stable, long-term population density is commonly estimated, but short-term and seasonally fluctuating densities are extremely challenging to measure and therefore difficult to quantify (*10*). Observations of cyclic (seasonal and multiennial) variations in pathogen incidence can provide an opportunity for evaluating the association between population density and transmission rates.

Although the dynamic implications of complex seasonal patterns have been studied thoroughly (*11*, *12*), the (biological or demographic) mechanism underlying seasonal fluctuations in incidence is often unknown (*6*, *7*). Here, we focus on biological mechanisms behind the seasonal cycles of measles in Niger. Directly transmitted, strongly immunizing childhood infections, such

[1]Department of Ecology and Evolutionary Biology, Princeton University, Princeton, NJ 08544, USA. [2]Center for Health and Wellbeing, Woodrow Wilson School of Public and International Affairs, Princeton University, Princeton, NJ 08544, USA. [3]Department of Geography, University of Florida, Gainesville, FL 32610, USA. [4]Emerging Pathogens Institute, University of Florida, Gainesville, FL 32610, USA. [5]Biology Department, Penn State University, University Park, PA 16802, USA. [6]Center for Infectious Disease Dynamics, Pennsylvania State University, University Park, PA 16802, USA. [7]Epicentre, 75011 Paris, France. [8]Harvard Humanitarian Initiative, Cambridge, MA 02138, USA. [9]Direction Générale de la Santé Publique (DGSP), Ministère de la Santé, Niamey, Niger. [10]Fogarty International Center, National Institutes of Health, Bethesda, MD 20892, USA.

*To whom correspondence should be addressed. E-mail: nbharti@princeton.edu

as measles, are the best-studied examples of the link between population density (e.g., aggregation in schools in industrialized countries) and seasonal disease transmission (*3*).

Recent measles epidemics in Niger show considerably stronger seasonal dynamics than the industrialized, prevaccination paradigm (*2*). Although the magnitude of outbreaks varies greatly between years, the timing is exceptionally consistent; outbreaks occur only during the annual dry season (*2*) (Fig. 1, A to C). Previous work has hypothesized that Niger's seasonal cycles of measles are caused by fluctuations in population density and contact rates, rather than schooling (*2*), consistent with the young median age of infection (~2 years). The economy and work force of Niger are largely agricultural, and seasonal relocation to low-density agricultural areas during the rainy season and to high-density urban areas during the dry season is common (*13*, *14*). Seasonal migration in this region, and in Niger specifically, has been documented, but sample sizes are often small, and the epidemiological implications of such movements are not fully understood (*14*).

Static estimates of the distribution of average population density can be obtained from national censuses, household surveys, and satellite imagery. One form of satellite imagery from the Defense Meteorological Satellite Program (DMSP) Operational Linescan System (OLS) detects nighttime light, which can be used to map settlements across large areas (*15*). Hundreds of nighttime images are composited to identify stable patches of electrification and domestic fires; bright areas on composites represent consistently detectable, relatively dense settlements (*15*, *16*). The serial images used to build such composites can reveal information about temporal changes in populations (*17*). Detecting seasonal changes in urban nighttime brightness allows us to quantify migration and to evaluate relative population density as a determinant of fluctuations in measles transmission.

Using a time series of DMSP OLS images, we measured serial values of urban brightness as a proxy for relative population density [details in supporting online material (SOM) part 1] in three cities in Niger. We compared seasonal patterns of population density, as measured by brightness, to seasonally varying measles transmission parameters, as estimated from 10 years of weekly reported measles cases (*1*). Last, we analyzed the spatiotemporal patterns of nighttime lights and measles incidence within the largest city of Niger.

Our analysis focused on three cities in Niger (Fig. 1A): Niamey, Maradi, and Zinder. Weekly measles incidence from 1995 to 2004 for these cities showed strong seasonal fluctuations (*2*). For each city, brightness values were extracted as unitless, digital numbers from 155 cloud-free, low lunar illumination images taken during 2000–2004 between 7 p.m. and 10 p.m. (fig. S1B).

The qualitative patterns of seasonal changes in brightness for all three cities were similar. Brightness fell below each city's mean during the rainy season and rose above its mean during the dry season (Fig. 1E and SOM part 1). Relative measles transmission rates [for biweekly time steps, estimated in (*1*)] and brightness were strongly positively correlated for all three cities (Fig. 1, D to F; table S1; and fig. S1; Pearson correlation = 0.88, 0.88, and 0.78 for Niamey, Maradi, and Zinder, respectively, $P < 0.01$ for all cities). In addition, the magnitude of the fluctuations in brightness and the transmission rates were similar; Maradi and Zinder had relatively low variance in brightness (0.07 and 0.07, respectively) and relatively low variance in transmission rate (0.14 and 0.12, respectively), whereas Niamey had higher variance in both brightness (0.22) and transmission rate (0.23).

The high spatial resolution of the images (~1 km) also allowed us to analyze spatial patterns of relative brightness within cities (see also SOM part 1). Within Niamey, measles cases were reported at the commune level during an outbreak in 2003–2004. These data provided an opportunity to test whether local fluctuations in population density correlated with measles incidence. Values for mean and range of brightness varied by commune (Fig. 2, A and B, and table S2). Measles incidence appeared and peaked earliest in commune 1, followed closely by commune 2, and considerably later in commune 3 (Fig. 2C). The observed pattern of brightness tracked the progression of measles through the communes (Fig. 2, B and C). Together, communes 1 and 2 experienced more than 90% of the reported cases in the city, which matched the relative magnitude of brightness by commune.

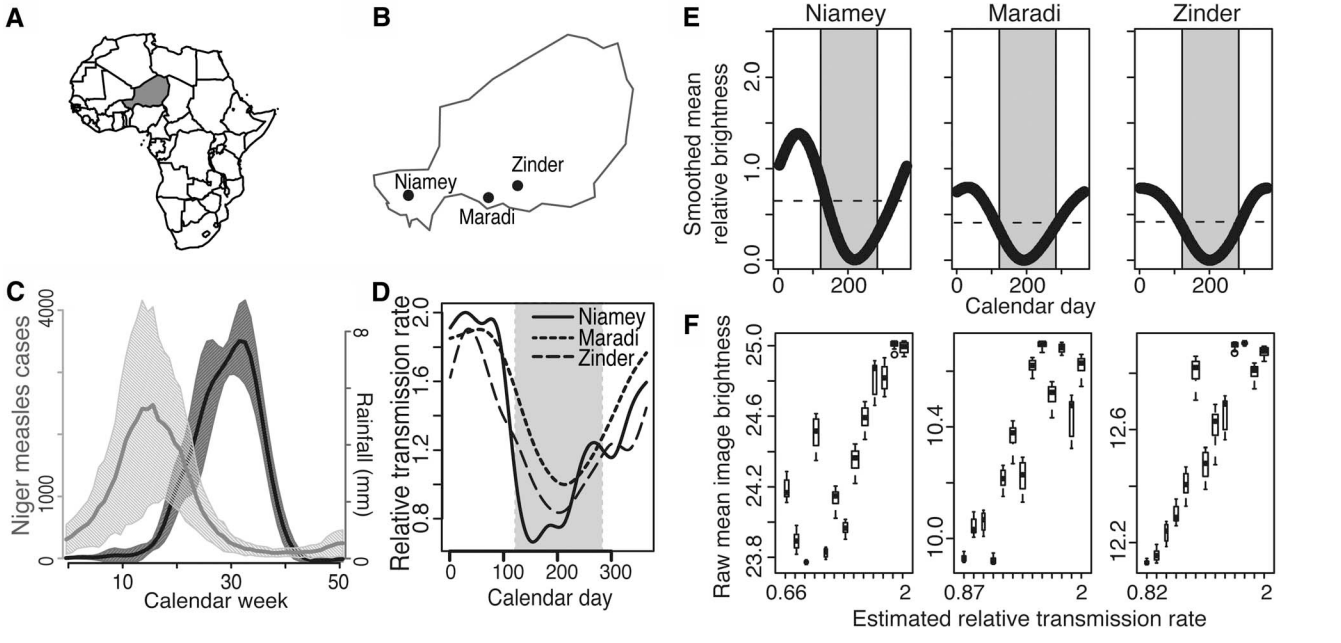

Fig. 1. (**A**) Map of Africa, Niger in gray. (**B**) Three cities of Niger included in this study. (**C**) Average weekly annual rainfall for Niger (dark gray) and national weekly average of annual measles cases, 1995–2004 (light gray). Shading gives 95% confidence intervals. (**D**) Relative transmission rates (number of infections per product of susceptible and infectious individuals per 2 weeks) for Niamey, Maradi, Zinder by calendar day 1 to 365 (*x* axis) (*1*). Gray area indicates rainy season. (**E**) Relative brightness (cubic smoothing spline, df = 3) by calendar day 1 to 365 (*x* axis) for each city. Gray area indicates rainy season; dashed line indicates mean of brightness for each city (table S1). (**F**) Brightness against relative transmission rate for each city. Box indicates interquartile range, whiskers extend 1.5 times the interquartile range. Width of boxes correlates to number of observations.

On day 161 of the epidemic, the Ministry of Health (MoH), the World Health Organization (WHO), and Médecins Sans Frontières began a 2-week outbreak response vaccination (ORV) within Niamey. The intervention began after the peak of the measles epidemic in communes 1 and 2 but before the peak in commune 3 (Fig. 2C). The brightness curves for each commune suggest that, at the onset of the vaccination campaign, population density was declining in communes 1 and 2 and increasing in commune 3 (Fig. 2B). Lags in reporting and stochasticity can complicate real-time predictions of epidemics. With this new information on changes in population density, we suggest that citywide interventions, both reactive and preventative, would increase coverage and impact if conducted during times of rising population density in the largest communes.

To assess the predictive power of brightness values for population density fluctuations within a city, we adapted a standard SEIR (susceptible-exposed-infectious-recovered) model to fit reported daily measles cases (*18*) using commune-level brightness in Niamey as a proxy for migration (details in SOM part 2). Seasonal variations in transmission rates are generally incorporated via a phenomenological, time-varying transmission parameter (β_t). This approach is implicitly based on static measures of population density (i.e., the number of hosts and the area occupied are assumed constant). For directly transmitted infections, β_t is a function of the dependence of contact rates on population density, and the probability that a contact between a susceptible (S) and an infected individual (I) will result in transmission (*19*). Each of these components can vary with time, but it is rarely explicit which contributes to time-varying transmission rates, β_t. By contrast, the SEIR model presented here includes a dynamic relative population size, where migration is modeled as a linear function (with slope Θ, see SOM part 2) of the derivative of brightness, independently for each commune. We fit two additional models for each commune: one with no migration and one with constant migration. Both were fit using the same methodology as the nighttime lights–informed model; the former was restricted to $\Theta = 0$, and for the latter, we fit a constant migration term that was independent of brightness.

Parameter values for β, migration rate (either Θ or nighttime lights–independent), and the initial susceptible population size (S_0) were fit simultaneously using a Bayesian particle filter (details in SOM part 2). For all three communes, the model with fluctuations in population size indexed by measurements of nighttime lights brightness fit the magnitude and actual timing of the observed measles epidemic best (Fig. 2D). This was particularly apparent in communes 1 and 2, where the bulk of the measles cases occurred. Nighttime lights–informed model predictions of measles incidence also captured the observed relative timing of the epidemic (SOM part 2), predicting that both the start and peak of the epidemic would progress in sequence from commune 1 to commune 2 to commune 3. The other two models failed to consistently capture this pattern.

Our results demonstrate that spatiotemporal fluctuations in brightness can explain the seasonality of measles outbreaks in urban areas of Niger, as well as the relative magnitude of seasonality. Within Niamey, explicit SEIR models show that the estimated fluctuations in population density, based on nighttime light brightness, explain the initial trajectory and overall magnitude of the epidemic within each commune. Migration has important epidemiological impacts (*20*, *21*), and we are now able to remotely detect the timing, location, and relative magnitude of these movements, as demonstrated here for three cities in Niger.

Previously developed measurements of population density provide high-resolution static estimates (*22*, *23*) or insight into long-term trends of changing populations (e.g., censuses). Mobile phone–usage records thoroughly describe short-term, individual movements of frequent mobile phone users (*24*) but do not necessarily approximate population density, especially in regions lacking resources. Although this level of detail would complement and strengthen population-level measures, its recent introduction, surge in subscribers, and proprietary and sensitive nature limit the current usability of mobile phone data as a primary resource for measuring changes in population density. In contrast, open-source nighttime light imagery detects decades of relatively high-resolution spatial and temporal changes in population density for assessing the fundamental scaling of disease transmission and density. Measurements of nighttime lights are most informative in areas of changing population density that produce detectable levels of anthropogenic light but are not so developed that brightness values are consistently saturated. These characteristics are consistent with some of the most disease-burdened regions of the world.

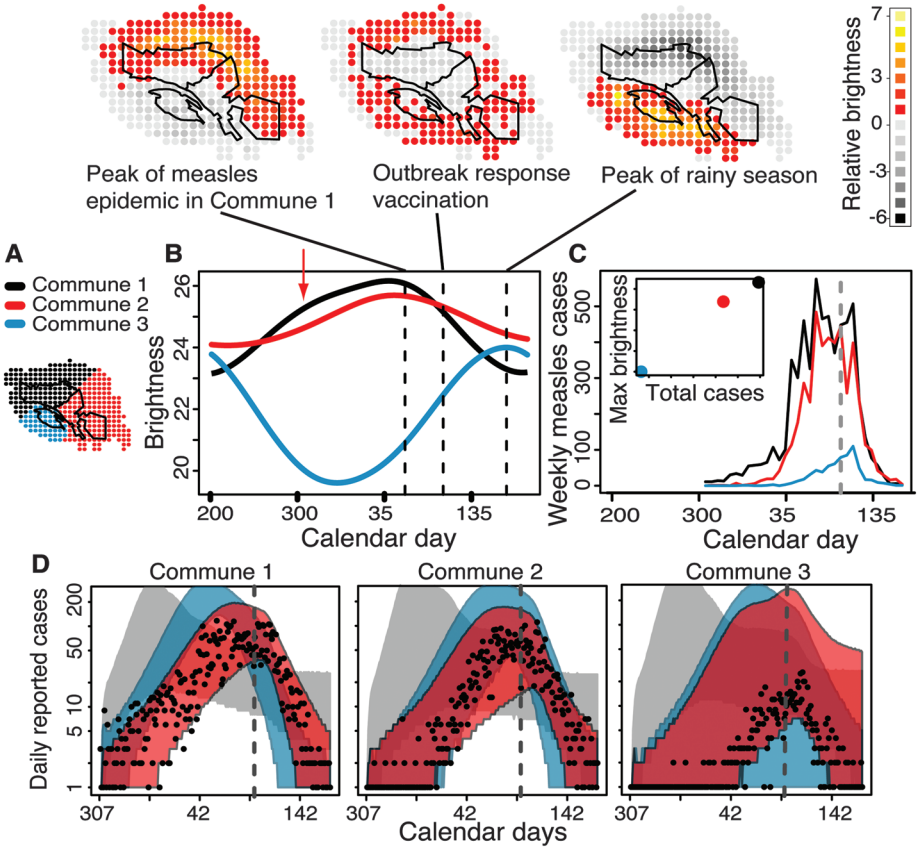

Fig. 2. (**A**) Pixels of Niamey designating communes by color, consistent for panels (A) to (C). Black polygons outline communes. (**B**) (Plot) Brightness (cubic smoothing spline, df = 3) for each commune from calendar day 200 (*x* axis). Red arrow indicates start of epidemic in commune 1. (Panels above and vertical lines) Colors indicate relative brightness of each pixel in Niamey at the peak of the epidemic in commune 1 (left), the onset of ORV (center), and the peak of rainy season (right). Mean of each pixel is set to zero. Black polygons outline communes. (**C**) Weekly reported measles cases by commune from calendar day 200. Dashed line represents timing of ORV. (Inset) Maximum brightness value of each commune against total measles cases. (**D**) Points show reported measles cases, shading gives central 95% of predicted measles incidence from 25000 model simulations from nighttime lights–informed model (red), no migration model (blue), and constant migration model (gray). Dashed line indicates timing of ORV. The *x* axis spans the duration of the epidemic: day 307 of 2003 to day 153 of 2004; the *y* axis is the number of cases on a natural log scale.

As with any method, there are limitations to the use of nighttime satellite imagery; the exact association between brightness and population density varies between locations and is affected by environmental (*15*) and economic factors (*25*–*27*). Additionally, images must be selected carefully to avoid contamination from solar and lunar illumination and cloud cover (SOM part 1).

Measuring the drivers of seasonal variability in transmission rates, particularly in areas with sparse disease surveillance and strong epidemic nonlinearities (*2*), is critical for improving the design of epidemiological control measures. It is now possible to improve outbreak response strategies based on fluctuations in population density and disease transmission, as we have shown for a recent measles outbreak in Niamey. This would be particularly useful in areas with repetitive seasonal fluctuations in density where targeted campaigns could maximize the number of individuals present during vaccinations. It is also possible that this method could be adapted for near–real-time analyses, as images are uploaded from the satellite within ~48 hours (although the usability of individual images is sensitive to environmental conditions).

The advantages of understanding changes in population density are broadly applicable. This information can aid in estimating population changes caused by large-scale human movements—i.e., displacement due to conflict (*17*) or recurring movements such as the Hajj. Measurements of fluctuations in population density provide important information to guide decisions on disease control strategies, international aid and humanitarian responses, and assessments of economic development.

References and Notes

1. M. J. Ferrari *et al.*, *Proc. Biol. Sci.* **277**, 2775 (2010).
2. M. J. Ferrari *et al.*, *Nature* **451**, 679 (2008).
3. W. P. London, J. A. Yorke, *Am. J. Epidemiol.* **98**, 468 (1973).
4. D. P. Word, J. K. Young, D. A. T. Cummings, D. C. Laird, paper presented at the 20th European Symposium on Computer Aided Process Engineering— ESCAPE20, Ischia, Naples, Italy, 6 to 9 June 2010.
5. S. S. Hutchins *et al.*, *Am. J. Epidemiol.* **132**, 157 (1990).
6. S. Altizer *et al.*, *Ecol. Lett.* **9**, 467 (2006).
7. N. C. Grassly, C. Fraser, *Proc. Biol. Sci.* **273**, 2541 (2006).
8. R. M. Anderson, R. M. May, *Infectious Diseases of Humans: Dynamics and Control* (Oxford Univ. Press, New York, 1991).
9. M. Keeling, P. Rohani, *Modeling Infectious Diseases in Human and Animals* (Princeton Univ. Press, Princeton, NJ, 2008).
10. R. M. Prothero, *Glob. Change Hum. Health* **3**, 20 (2002).
11. J. L. Aron, I. B. Schwartz, *J. Theor. Biol.* **110**, 665 (1984).
12. M. J. Keeling, B. T. Grenfell, *Science* **275**, 65 (1997).
13. R. H. Faulkingham, P. F. Thorbahn, *Popul. Stud.* **29**, 463 (1975).
14. D. Rain, *Eaters of the Dry Season: Circular Labor Migration in the West African Sahel* (Westview Press, Boulder, CO, 1999).
15. C. D. Elvidge, K. E. Baugh, E. A. Kihn, H. W. Kroehl, E. R. Davis, *Photogramm. Eng. Remote Sensing* **63**, 734 (1997).
16. P. Sutton, D. Roberts, C. D. Elvidge, K. E. Baugh, *Int. J. Remote Sens.* **22**, 3061 (2001).
17. J. Agnew, T. W. Gillespie, J. Gonzalez, B. Min, *Environ. Plan. A* **40**, 2285 (2008).
18. R. F. Grais *et al.*, *Trans. R. Soc. Trop. Med. Hyg.* **100**, 867 (2006).
19. M. Begon *et al.*, *Epidemiol. Infect.* **129**, 147 (2002).
20. K. R. Yaméogo *et al.*, *Int. J. Epidemiol.* **34**, 556 (2005).
21. M. C. C. Camargo, J. C. de Moraes, V. A. U. F. Souza, M. R. Matos, C. S. Pannuti, *Rev. Panam. Salud Publica* **7**, 359 (2000).
22. D. Balk *et al.*, *Adv. Parasitol.* **62**, 119 (2006).
23. J. Dobson, E. Bright, P. R. Coleman, R. Durfee, B. Worley, *Photogramm. Eng. Remote Sensing* **66**, 849 (2000).
24. M. C. González, C. A. Hidalgo, A. L. Barabási, *Nature* **453**, 779 (2008).
25. A. Noor, V. Alegana, P. Gething, A. Tatem, R. Snow, *Popul. Health Metr.* **6**, 5 (2008).
26. S. Ebener, C. Murray, A. Tandon, C. C. Elvidge, *Int. J. Health Geogr.* **4**, 5 (2005).
27. C. D. Elvidge *et al.*, *Comput. Geosci.* **35**, 1652 (2009).

Acknowledgments: This study was supported by the Bill and Melinda Gates Foundation. A.J.T. is supported by a grant from the Bill and Melinda Gates Foundation (49446). A.J.T., M.J.F., and B.T.G. are also supported by the Research and Policy for Infectious Disease Dynamics (RAPIDD) program of the Science and Technology Directorate, Department of Homeland Security and the Fogarty International Center, NIH. All DMSP OLS imagery is available from the Space Physics Interactive Data Resource (http://spidr.ngdc.noaa.gov/spidr/).

Supporting Online Material

www.sciencemag.org/cgi/content/full/334/6061/1424/DC1
Materials and Methods
SOM Text
Figs. S1 to S3
Tables S1 to S4
References (*28*–*40*)

1 July 2011; accepted 21 October 2011
10.1126/science.1210554

Empathy and Pro-Social Behavior in Rats

Inbal Ben-Ami Bartal,[1] Jean Decety,[1,2,4] Peggy Mason[3,4]

Whereas human pro-social behavior is often driven by empathic concern for another, it is unclear whether nonprimate mammals experience a similar motivational state. To test for empathically motivated pro-social behavior in rodents, we placed a free rat in an arena with a cagemate trapped in a restrainer. After several sessions, the free rat learned to intentionally and quickly open the restrainer and free the cagemate. Rats did not open empty or object-containing restrainers. They freed cagemates even when social contact was prevented. When liberating a cagemate was pitted against chocolate contained within a second restrainer, rats opened both restrainers and typically shared the chocolate. Thus, rats behave pro-socially in response to a conspecific's distress, providing strong evidence for biological roots of empathically motivated helping behavior.

Pro-social behavior refers to actions that are intended to benefit another. One common motivator of pro-social behavior in humans is empathic concern: an other-oriented emotional response elicited by and congruent with the perceived welfare of an individual in distress (*1*, *2*). Sharing another's distress via emotional contagion can result in overwhelming fear and immobility unless one's own distress is down-regulated, thus allowing empathically driven pro-social behavior (*3*, *4*). Building on observations of emotional contagion in rodents (*5*–*10*), we sought to determine whether rats are capable of empathically motivated helping behavior. We tested whether the presence of a trapped cagemate induces a pro-social motivational state in rats, leading them to open the restrainer door and liberate the cagemate.

[1]Department of Psychology, University of Chicago, Chicago, IL, USA. [2]Department of Psychiatry and Behavioral Neuroscience, University of Chicago, Chicago, IL, USA. [3]Department of Neurobiology, University of Chicago, Chicago, IL, USA. [4]Committee on Neurobiology, University of Chicago, Chicago, IL, USA.

Rats were housed in pairs for 2 weeks before the start of testing. In each session, a rat (the free rat) was placed in an arena with a centrally located restrainer in which a cagemate was trapped (trapped condition, $n = 30$ rats, 6 females). The free rat could liberate the trapped rat by applying enough force to tip over the restrainer door (Fig. 1A). If a free rat failed to open the door, the experimenter opened it halfway, allowing the trapped rat to escape and preventing learned helplessness. Rats remained in the arena together for the final third of the session. Door-opening only counted as such if the free rat opened the door before the experimenter opened it halfway. Sessions were repeated for 12 days. Control conditions included testing a free rat with an empty restrainer (empty condition, $n = 20$ rats, 6 females) or toy rat–containing restrainer (object condition, $n = 8$ males). As an additional control, for the number of rats present, we tested a free rat with an empty restrainer and an unrestrained cagemate located across a perforated divide (2+empty condition, $n = 12$ males). Free rats' heads were marked and their movements were recorded with a top-mounted camera for offline analysis (*11*).

Free rats circled the restrainer, digging at it and biting it, and contacted the trapped rat through holes in the restrainer (Fig. 1B and movie S1). They learned to open the door and liberate the trapped cagemate within a mean of 6.9 ± 2.9 days. Free rats spent more time near the restrainer in